Perturbed angular correlation measurements of ^{111}Cd in cobalt (II, III) oxide

1991 J. Phys.: Condens. Matter 3 2137

(http://iopscience.iop.org/0953-8984/3/13/016)

J. Phys.: Condens. Matter 3 (1991) 2137–2145. Printed in the UK

Perturbed angular correlation measurements of ^{111}Cd in cobalt (II, III) oxide

Z Inglot and D Wegner
II. Physikalisches Institut, Universität Göttingen and Sonderforschungsbereich 126, Göttingen/Clausthal D-3400 Göttingen, Federal Republic of Germany

Received 17 April 1990, in final form 4 December 1990

Abstract. The time differential perturbed angular correlation of ^{111}Cd has been measured after implantation of the radioactive mother isotope ^{111}In into Co_3O_4. Besides a broad distribution of electric field gradients ($\langle\nu_{QC}\rangle = 105(5)$ MHz, $\eta_C = 0.8(1)$) two fractions with $\nu_{QA} = 0$ and $\nu_{QB} = 145$ MHz, $\eta_B < 0.15$ are found which have been associated with ^{111}In on substitutional A and B sites of the spinel lattice. During isochronal annealings at various oxygen partial pressures, the distribution widths δ_A and δ_B and the asymmetry parameter η_B approach zero; simultaneously, ν_{QB} slightly decreases. The changes are correlated and quantitatively explained in the point charge model.

1. Introduction

In recent papers [1–3] we reported on perturbed angular correlation (PAC) studies on the first oxidation stages of CoO to Co_3O_4. We observed the incorporation and agglomeration of cation vacancies in up to three-dimensional complexes with spinel-like microstructures. We also presented first results of PAC experiments on the reduction of Co_3O_4 and found similar PAC spectra for $Co_{1-\Delta}O$, $\Delta > 0$ and $Co_{3-\Delta}O_4$, $\Delta < 0$ indicating similar environments of the ^{111}Cd probes.

This work is aimed at the clarification of the nature of ^{111}In sites after implantation in Co_3O_4, and at the understanding of microphysical processes observed during isochronal annealing programmes at various oxygen partial pressures. Literature data on the defect chemistry of Co_3O_4 are scarce. Thus, the interpretation will mainly refer to electric field gradient (EFG) calculations in the point charge model (PCM) based upon the well known lattice structure of the Co_3O_4 spinel [4].

In the following section we will briefly describe the PAC method and the sample treatments. After presentation of the experimental results, we will outline the PCM calculations and discuss them in comparison with the experimental findings.

2. Experimental

2.1. PAC method and apparatus

The PAC probe nucleus ^{111}Cd is populated by the electron capture of ^{111}In (half life $T_{1/2} = 2.8$ days) followed by the $\frac{7}{2}^+ \rightarrow \frac{5}{2}^+ \rightarrow \frac{1}{2}^+$ nuclear transitions to the ^{111}Cd ground

0953-8984/91/132137 + 09 $03.50

state. If the quadrupole moment Q of the isomeric $\frac{5}{2}^+$ level interacts with an EFG, the angular correlation of the two successively emitted γ-quanta is perturbed. Consequently, the correlation function is modulated with a time-dependent perturbation factor

$$G_2(t) = \sum s_{2n}(\eta) \cos(g_n(\eta)\nu_Q t) \exp(-g_n(\eta)\delta t).$$

Here, δ is the width of a Lorentzian distribution around ν_Q, $s_n(\eta)$ and $g_n(\eta)$ are functions of the EFG asymmetry parameter η. This parameter is defined via $\eta = (V_{xx} - V_{yy})/V_{zz}$ where V_{ii} are the elements of the diagonalized EFG tensor with the setting $|V_{zz}| \geqslant |V_{yy}| \geqslant |V_{xx}|$. Because of the Laplace equation $V_{xx} + V_{yy} + V_{zz} = 0$ the EFG tensor is completely defined by η and V_{zz}. The latter enters into the quadrupole frequency: $\nu_Q = eQV_{zz}/h$. If several fractions f_i are present, the perturbation function $G(t) = \sum f_i G_2^{(i)}(t)$ with $\sum f_i = 1$ is extracted from the function

$$R(t) = 2\frac{N(\pi, t) - N(\pi/2, t)}{N(\pi, t) + 2N(\pi/2, t)} = A_{22}^{\text{eff}} G(t)$$

where $N(\Theta, t)$ denotes the background corrected coincidence spectrum obtained with two detectors positioned at the respective angles $\Theta = \pi/2$ and π. A_{22}^{eff} is the effective anisotropy coefficient of the $\gamma - \gamma$ cascade corrected for finite detector size and solid angle. For ^{111}Cd, the relevant numbers are $A_{22} = -0.176$, $A_{22}^{\text{eff}} \approx -0.13$, $Q = 0.83$ b; the lifetime of the isomeric state is $\tau = 122$ ns [5].

The coincidence spectra were measured with a conventional slow–fast detector set up consisting of four NaJ(Tl) detectors. Four spectra with $\Theta = \pi$ and eight with $\Theta = \pi/2$ were recorded simultaneously. The geometrical average of equivalent combinations entered into the $R(t)$ algorithm. The total time resolution was 3.9 ns (FWHM).

2.2. *Sample treatments*

The Co_3O_4 powder of 99.9985% metallic purity (Ventron Alfa Produkte) was pressed on aluminium or nickel foils. The ^{111}In activity was introduced by means of the Göttingen heavy ion implanter IONAS [6]. With an implantation energy of 450 keV, a dose of 10^{11} atoms at an average depth of 80 nm was obtained. The maximum concentration of ^{111}In in the implantation profile is lower than 10^{-4}.

Isochronal annealing programmes up to 800 K or 1073 K were performed at oxygen partial pressures of 0.2 Pa, 0.2 kPa and 2 kPa. The duration of each annealing step was 15 min, each followed by a PAC measurement.

3. Results

All measured hyperfine parameters are collected in table 1. The perturbation function of the as-implanted samples is characterized by three contributions labelled A, B and C (figure 1(*a*)). Only one of them (B) exhibits a quite sharp EFG with $\nu_{QB} = 146$ MHz, $\eta_B = 0.15$, $\delta_B = 5.5$ MHz and a fraction $f_B \approx 45\%$. The other two perturbations are due to broad EFG distributions: $\langle \nu_{QA} \rangle = 0$, $\delta_A = 30(10)$ MHz and $\langle \nu_{QC} \rangle = 105(5)$ MHz, $\eta_C = 0.8(1)$, $\delta_C = 30(10)$ MHz. With one exception (see below), these three fractions are sufficient to describe all $R(t)$ functions obtained in the course of the annealing programmes. Figure 1(*a*) gathers three typical $R(t)$ functions and their Fourier transforms measured in the as-implanted state and after annealings at $T_a = 600$ K and

Table 1. Hyperfine parameters of ^{111}Cd in Co_3O_4.

Fraction	ν_Q (MHz)	η	δ (MHz)
A	0	—	<25
B	145–147	<0.15	<5.6
C	105(10)	0.8(1)	25(10)
D	92(3)	<0.1	6(1)

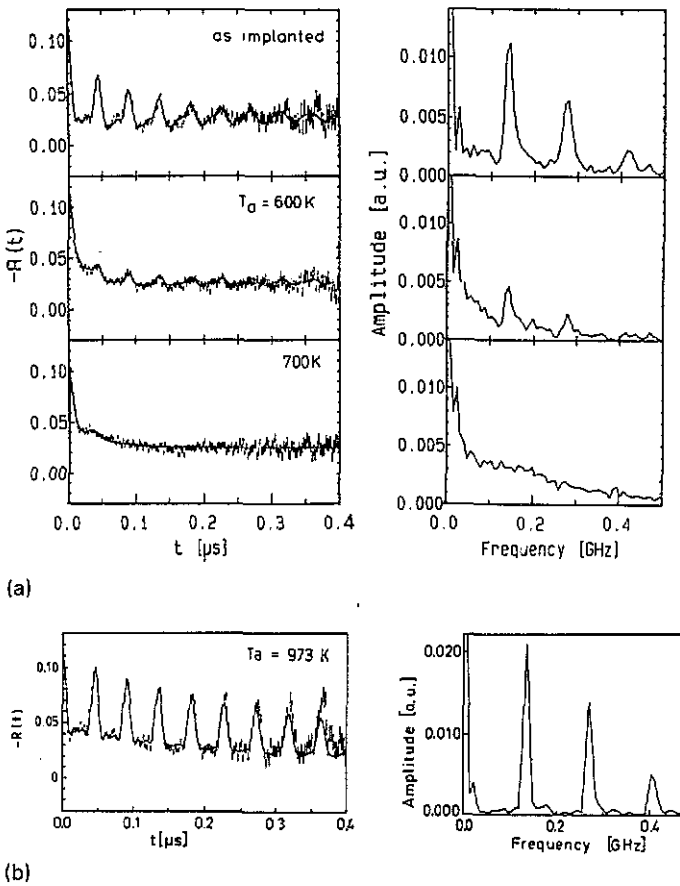

Figure 1. (*a*) Typical $R(t)$ functions and their Fourier transforms of ^{111}Cd in Co_3O_4 observed in the course of an isochronal annealing programme at $p(O_2) = 0.2$ Pa. (*b*) Perturbation function $R(t)$ and corresponding Fourier transform of ^{111}Cd in Co_3O_4 taken after annealing at 973 K and $p(O_2) = 2$ kPa.

700 K at $p(O_2) = 0.2$ Pa. Figure 2 shows the fractions f_i as a function of the annealing temperature T_a for the three oxygen partial pressures $p(O_2) = 0.2$ Pa, 0.2 kPa and 2 kPa. f_B stays constant until it drops down at pressure-dependent temperatures which are 550 K (0.2 Pa), 1000 K (0.2 kPa) and 1100 K (2 kPa), respectively. Hyperfine parameters of fraction B undergo small but significant changes: δ_B decreases to less than 1 MHz, η_B

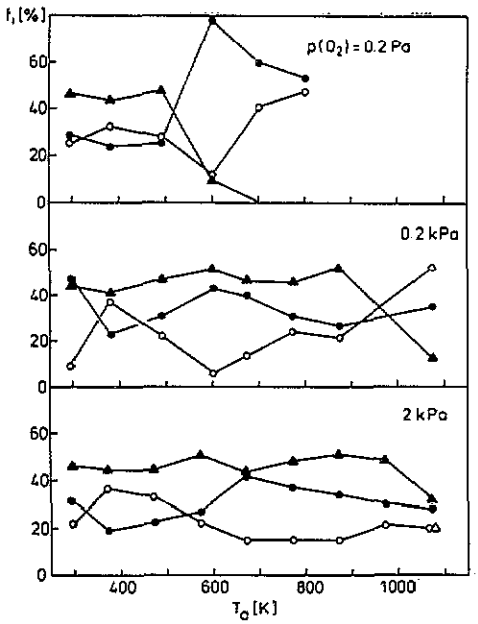

Figure 2. Fractions f_A(●), f_B(▲), f_C(○) and f_D(△) as function of the annealing temperature T_a for various oxygen partial pressures.

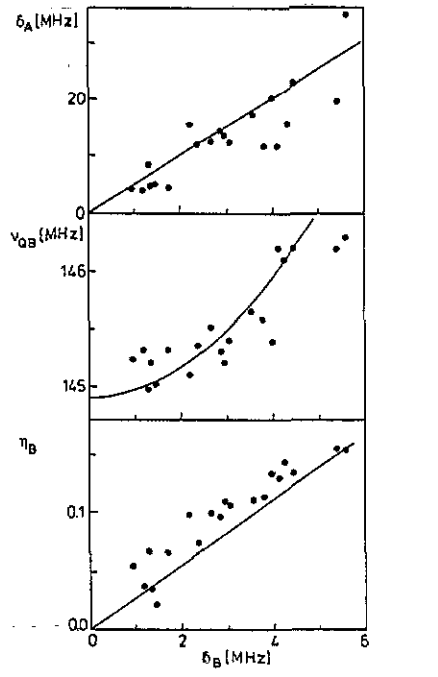

Figure 3. Correlations between δ_B, η_B, ν_{QB} and δ_A presented as functions of δ. The line is calculated (section 4.2).

to 0.04 (figure 1(*b*)) and ν_{QB} is diminished by approximately 1.5 MHz. All variations are correlated as shown in figure 3, where η_B and ν_{QB} are plotted against δ_B.

Fraction f_A exhibits a maximum at $T_a \approx 600$ K, irrespective of the oxygen pressure. The distribution width δ_A decreases with increasing temperature. All obtained δ_A values are plotted against δ_B in figure 3 and again a correlation is found. For explanation of the lines in figure 3 see section 4.2.

Finally, f_C has a more or less clear minimum at about $T_a = 600$ K. δ_C varies considerably between 20 and 100 MHz, but in a non-systematic way. $\langle \nu_{QC} \rangle$ is quite constant. It might be interesting to note that the fundamental frequencies $\omega = g_1(\eta)\nu_Q$ are similar for B and C. This was the reason for attributing f_C to a strongly distorted B environment [1]. f_B is mainly transformed to f_A at $p(O_2) = 0.2$ Pa, to f_C at 0.2 kPa and to a new fraction ($\nu_{QD} = 92$ MHz, $\eta = 0$) at 2 kPa. In the last case f_D vanishes and f_B is restored to 70% by oxidation of the sample in air at 770 K.

4. Discussion

We would like to discuss the following questions:

(i) To which structural microsurroundings should the perturbations be attributed?

(ii) How can the correlations of the hyperfine parameters δ_A, δ_B, η_B and ν_{QB} be understood?

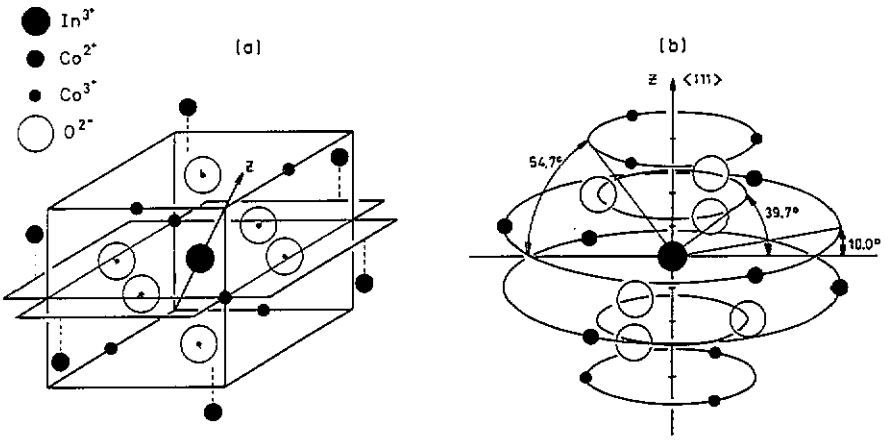

Figure 4. Next-neighbour A, B and O ions of a spinel B site. The O ions are relaxed from the face centres along (111) by 0.18 Å. The arrangement is displayed with respect to the cubic system (*a*) and the (111) symmetry axis (*b*).

(iii) What physico-chemical processes cause the variation of fractions in the annealing programme?

4.1. Interpretation of perturbations

Co_3O_4 forms a normal spinel lattice, i.e. the tetrahedrally coordinated A sites are occupied by Co^{2+} ions and the octahedral B sites by Co^{3+} ions [4]. The O^{2-} ions are arranged in a slightly distorted FCC structure. Each of them is coordinated by three B and one A ion and relaxed towards the base of the B_3A pyramid by 0.18 Å (figure 4(*a*)). One has to expect that implanted In ions, at least partially, come to rest on substitutional lattice sites. From that point of view it is interesting to compare the measured hyperfine parameters with results from other experiments and EFG calculations.

The symmetry of the A sites suggests a vanishing EFG. This is confirmed by the results of PAC experiments on Fe_3O_4 by Asai *et al* [7] who measured a pure magnetic hyperfine interaction below the Néel temperature. Mössbauer studies of various spinels [8] also prove the absence of A-ion electric quadrupole interactions. Thus, we associate the fraction f_A with the population of the corresponding spinel sites. The EFG distribution width decreasing with increasing annealing temperature is attributed to random lattice defects caused by implantation damage and/or thermodynamical deviation from the ideal stoichiometry. Furthermore, we propose that f_B corresponds to ^{111}In ions on the spinel B sites. Spencer and Schroeer [8] found finite EFG in various spinels, among them Co_3O_4. The quadrupole splitting of the Mössbauer isotope ^{57}Co in Co_3O_4 was 0.54 mm s^{-1}. With respect to the quadrupole moment $Q_{Fe} = 0.08$ b [9] and the anti-shielding factor $(1 - \gamma\infty)_{Fe} = 10.64$ of Fe^{3+} [10] we obtain a $V_{zz} = 6.0 \times 10^{20}$ V m^{-2}. The quadrupole frequency $\nu_{QB} = 145$ MHz measured here yields $V_{zz} = 2.4 \times 10^{20}$ V m^{-2} with $(1 - \gamma\infty)_{Cd} = 30.27$ [11].

Attempting to calculate ν_{QB} in the PCM, we arrive at some problems. Figure 4(*a*) sketches the next-neighbour shell of a Cd ion on a B site. The arrangement is redrawn in figure 4(*b*) with respect to the rotational symmetry axis along the ⟨111⟩ orientation. From the figure it follows that each sub-shell contributes to the axially symmetric EFG at

Table 2. EFG V_{zz} and quadrupole frequencies $\nu_Q = |(1 - \gamma\infty)eQV_{zz}/h|$ of ^{111}Cd on a Co_3O_4 B site caused by the next neighbour's Co^{2+} (A), Co^{3+} (B) and O^{2-} (O) PC. The angle θ is measured with respect to the (111) plane perpendicular to the EFG z axis.

PC	θ (deg)	V_{zz} (10^{20} V m^{-2})	ν_Q (MHz)
A	10.02	−4.20	255
B	54.74	11.19	680
O	39.70	−5.49	334
A + B + O	—	1.50	91

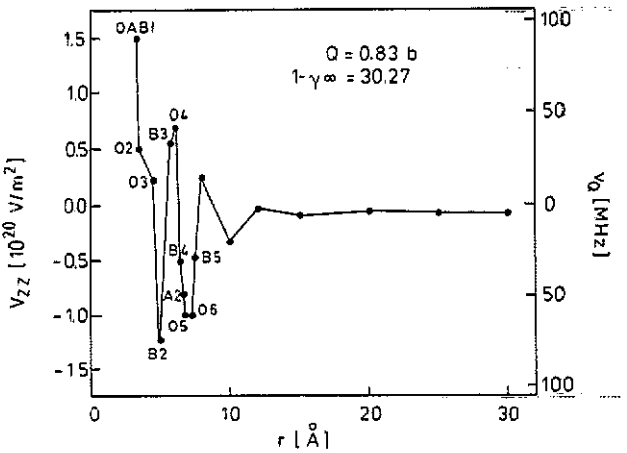

Figure 5. EFG at a B site in Co_3O_4 calculated in the PC model as function of the considered sphere radius r. The inserts X_n denote the nth shell of X ions.

the Cd site. The high EFG of the B sub-shell is nearly cancelled by the negative contribution of the A and relaxed O^{2-} ions, as can be seen from table 2. According to figure 5, the PC quadrupole frequency approaches zero if the calculation sphere is enlarged to more than 12 Å. Therefore, we suggest that the EFG is determined mainly by next-neighbour interactions in agreement with the suitability of cluster calculations [12]. There is a large contribution to the EFG due to the relaxation of the O^{2-} ions. In the non-relaxed case the oxygen coordination has cubic symmetry. The angle θ to the (111) plane would then be 35.3° and the EFG from the oxygen ions would vanish. Consequently, the quantitative EFG calculation has to be considered as quite speculative because a relaxation angle of 1° changes ν_{QB}^{PC} by 77 MHz. In this frame, agreement between the measured and the calculated values of ν_{QB} is obtained with $\theta = 39.0°$ (EFG > 0) and $\theta = 42.8°$ (EFG < 0).

We do not know anything about the lattice relaxation caused by the large size of the Cd^{2+} ion (radius 0.97 Å) compared with the Co^{3+} ion (radius 0.63 Å), but we will arrive at some new arguments in the discussion of the hyperfine parameter correlations.

Finally, perturbation C remains unclear. The unsystematic changes of δ_C do not allow well-founded conclusions, but suggest that they probably hide more than one fraction. Possible interpretations are strongly disturbed B sites and Cd ions located as interstitials or at grain boundaries.

One could suggest that the impurity In^{3+} ions are distributed randomly on the A and B sites of the spinel lattice corresponding to a ratio of $f_A:f_B = 1:2$. That would mean that the fitted fractions of the broadly distributed frequencies are not reliable. We checked this hypothesis and found, by fitting with the above constraint, a significantly worse χ^2 and a totally unsystematical variation of all parameters belonging to the third fraction. Thus, we have shown that the distribution of In^{3+} ions on the non-equivalent spinel sites is not random (in agreement with [13]) but depends on the thermodynamic state of the oxide.

4.2. *Correlations of hyperfine parameters*

As outlined in section 3, the PAC parameters δ_B, η_B and ν_{QB} vary in the course of the annealing programmes in a correlated way (see figure 3). Qualitatively, this fact can easily be understood. The ideal EFG ($\nu_{QB} = 145$ MHz) is disturbed by random defects in the sensitivity range of the PAC probe. This affects all three hyperfine parameters mentioned above. The strength of such an effect has been investigated by Forker [14] who assumed Gaussian EFG distribution widths Δ around V_{zz}^0 and η_0 and monitored the parameters δ, V_{zz} and η obtained from a fit of the averaged calculated perturbation functions. Indeed, he found considerable effects, e.g. for $\Delta/V_{zz} = 10\%$ and $\eta_0 = 0$ he received the fit result $\delta/V_{zz} = 0.1$, $\eta = 0.12$ and $V_{zz} = 1.01\ V_{zz}^0$. A comparison with the correlations presented in this work shows that there exists a considerable quantitative discrepancy. For $\delta_B/\nu_{QB} = 3.8\%$ we have $\eta_B = 0.16$ and $\Delta\nu_{QB}/\nu_{QB} = 1\%$. The deviation from the model calculation cannot be attributed to the Lorentzian distribution type used in this work.

In the following we present a simple quantitative model which explains our experimental findings. The basic idea is that the EFG of a random lattice defect is mainly transferred via the next-neighbour oxygen ions to the PAC nucleus, due to the polarization of the O^{2-} 2p orbitals which overlap with the ^{111}Cd 5s wave function. (A similar idea explained the super-transfer of magnetic hyperfine fields to ^{111}Cd in the antiferromagnets CoO, MnO and NiO [15].) A certain random defect may produce an EFG with the strength W at the PAC nucleus and this changes the ideal lattice EFG with $V_{zz}^0 < 0$ and $\eta_0 = 0$. Diagonalization of the resulting EFG tensor gives, with sufficiently small W:

$$V_{zz} = X/4 + 3Y/4 \qquad \eta = 3|(X - Y)/(X + 3Y)|$$

with

$$X = V_{zz}^0 + W \qquad Y = ((V_{zz}^0)^2 - 2V_{zz}^0 W\cos 2\theta + W^2)^{1/2}$$

where θ is the angle between the point charge and the x–y plane of the undisturbed EFG V_{zz}^0. The z axis of the EFG is turned by the angle

$$\varphi = \text{arcctg}[W\sin 2\theta/(V_{zz} - W\cos 2\theta + Y)].$$

It is clear that V_{zz} and η strongly depend on θ. If V_{zz} and η were averaged over θ and a Gaussian distribution of W, one should obtain similar results to those of Forker [14].

Our method here is different. A Lorentzian distribution of width δ around V_{zz}^0 is described by

$$P(V_{zz}) = \delta/\pi[\delta^2 + (V_{zz} - V_{zz}^0)^2]$$

so that

$$P(V_{zz}^0 \pm \delta) = \tfrac{1}{2}P(V_{zz}^0).$$

Vice versa, we have

$$V_{zz}^0 = (P_+^{-1}\tfrac{1}{2} + P_-^{-1}\tfrac{1}{2})/2$$

and

$$\delta = (P_+^{-1}\tfrac{1}{2} + P_-^{-1}\tfrac{1}{2})/2$$

where $P_{+,-}^{-1}$ denotes the inverse function of $P(V_{zz})$ with function value $V_{zz} > V_{zz}^0$ and $V_{zz} < V_{zz}^0$, respectively. (The same arguments apply to the two other components of the EFG tensor.) The model treats a Lorentzian distribution as a balance of two EFG centres with lever length δ. This simplification allows us to estimate how the change of an axially symmetric EFG induced by an EFG distribution of width δ_A acting with an angle δ can be calculated. We assume that $\delta_A = W$ is due to random defects in the lattice and monitored in our PAC measurements by ^{111}Cd ions on A sites. Then the EFG transfer angle θ is the only free parameter. Comparison with the experimental correlations for the hyperfine parameters of perturbation B in figure 3 yields $\theta \approx 43°$. The corresponding dependences between δ_A, δ_B, $\Delta\nu_{QB}$ and η_B are inserted as lines. With respect to the simplicity, the agreement with the experiments is quite nice, especially as the calculations by Forker [14] do not apply in our case.

In the foregoing section we noted that the PC EFG at B sites in the spinel lattice strongly depends on the angle θ of the oxygen ions with respect to the (111) plane. We found agreement between experimental and PC values of ν_{QB} for $\theta = 37.0°$ and $\theta = 42.8°$. The results of this section clearly favour the second possibility. The structure of the lattice (figure 4) suggests a relaxation along the ⟨111⟩ axis parallel to the EFG symmetry axis because the next octahedral site in this direction is empty.

4.3. Annealing behaviour

In this section the variations of the fractions with the annealing temperature are discussed. From figure 2 it is clear that the behaviour observed at different oxygen partial pressures is very similar. For all three oxygen activities f_c reaches a minimum value around $T_a = 600$ K. From this independency and the quite low activation energy we argue that the underlying process is the recombination of implantation-induced Frenkel pairs, i.e. mainly short range migration of interstitial atoms.

The most striking change in the annealing curves is the dropping in f_B at pressure-dependent temperatures. A comparison with the Co–O phase diagram [16] shows that this occurs 100 K ($p(O_2) = 2$ kPA) to 350 K (0.2 Pa) below the respective Co_3O_4/CoO phase equilibrium temperatures. One should expect that Co_3O_4 is reduced to CoO by desorption of oxygen at the surface and incorporation of Co interstitials, which is the reverse of the CoO oxidation mechanism [1, 17]. On the other hand, it is known that the spinel stores excess oxygen at the surface and grain boundaries according to the formula $Co_3O_{4+\varepsilon}$ [18]. (The existence of cationic vacancies ($Co_{3-\Delta}O_4$) is excluded by the study of sensitive bulk properties.) Consequently, it is not reasonable to assume the above

reduction mechanism, at least in the sense that a homogeneous concentration of Co interstitials is introduced with increasing temperatures. From our experiments we are not able to define one process as being responsible for the decrease of f_B. Figure 2 shows that f_B in one case is transformed to f_A (0.2 Pa), in a second case to f_C (0.2 Pa) and finally to a new fraction f_D (2 kPA). As the decrease of f_B is taken as a sign of the beginning dissociation of Co_3O_4, the denotations of the remaining fractions have to be considered with care. As long as the hyperfine parameters do not change we do not see any reason to choose additional labels, but it might be possible that serious variations of the probe surroundings are not reflected in the hyperfine parameters. For example, any cubic environment causes $\nu_Q = 0$. Thus, the PAC results allow different interpretations for each of the given oxygen partial pressures. One possible explanation could be the segregation into the two microphases CoO and Co_2O_3 which occurs, more or less completely, depending on the respective transition temperatures.

5. Summary

PAC measurements with ^{111}In as implanted and after annealing have been conducted on the spinel Co_3O_4. Three different fractions have been found, two of which are associated with occupations of the A and B lattice sites. This interpretation is confirmed by comparison with other experiments and with point charge calculations which correlate the distribution widths δ_A and δ_B and the hyperfine parameters ν_{QB} and η_B quantitatively.

Acknowledgments

We are indebted to Dr M Uhrmacher and D Purschke for the ^{111}In implantations.

References

[1] Wegner D, Inglot Z and Lieb K P 1990 *Ber. Bunsenges. Phys. Chem.* **94** 1
[2] Wegner D, Inglot Z and Lieb K P 1989 *8th Int. Conf. on Hyperfine Interactions (Prague); Hyperfine Interact.* **59** 313
[3] Inglot Z, Wegner D and Lieb K P 1990 *Proc. 24th Zakopane School on Physics (Poland)* ed J Stanek and A Pedziwiatr (Singapore: World Scientific) p 300
[4] Roth W L 1964 *J. Phys. Chem. Solids* **25** 1
[5] Herzog P, Freitag K, Reuschenbach M and Walitzki H 1980 *Z. Phys.* A **294** 13
[6] Uhrmacher M, Pampus K, Bergmeister F J, Purschke D and Lieb K P 1985 *Nucl. Instrum. Methods; Phys. Rev.* B **9** 234
[7] Asai K, Okeda T and Sekizawa H 1985 *J. Phys. Soc. Japan* **54** 4325
[8] Spencer C D and Schroeer D 1974 *Phys. Rev.* B **9** 3658
[9] Rafailovich M H, Dafni E, Brennan J M and Sprouse G D 1983 *Phys. Rev.* C **27** 602
[10] Barberan N, Tasker P W and Stoneham A M 1979 *J. Phys. C: Solid State Phys.* **12** 3827
[11] Feiock F D and Johnson W R 1969 *Phys. Rev.* **187** 39
[12] Nagel S 1985 *J. Phys. Chem. Sol.* **46** 743
[13] Fagherazzi G and Garbassi F 1971 *J. Appl. Crystallogr.* **5** 18
[14] Forker M 1973 *Nucl. Instrum. Methods* **106** 121
[15] Rinneberg H H and Shirley D A 1976 *Phys. Rev.* B **13** 2138
[16] Dieckmann R 1977 *Z. Phys. Chem., NF* **107** 13
[17] Nowotny J, Nowotny J T, Rekas M, Sadowski A and Twardosz M 1977 *Z. Phys. Chem., NF* **104** 155
[18] Tyuliev G and Angelov S 1988 *Appl. Surf. Sci.* **32** 381